Res. Rep. Fac. Eng. Mie Univ., Vol. 25, pp. 27−44 (2000)

Original Paper

Scale Effect on Compression Behavior of Concrete-Filled Steel Tube Short Columns

Takamasa YAMAMOTO, Jun KAWAGUCHI, Shosuke MORINO
Keiji YAMAMOTO and Yasunori MIZUNO
(Department of Architecture)

(Received September 18, 2000)

Abstract

Compression tests of concrete-filled steel tube (CFT) short columns have been conducted to clarify the scale effect on the compression behavior of CFT short columns. The experimental variables were as follows: shape of tube, size of specimen, strength of filled-concrete, *D/t* or *B/t* ratio, and loading method (applying the compression load only on the filled-concrete and on the overall cross-section). This paper first presents the test results concerning failure mode, circumferential strain distributions, load-deformation behavior, and discusses the evaluation of the strength of confined concrete inside the tube and the evaluation of the strength of CFT short columns considering the scale and confining effects.

Key words

CFT, Size of Specimens, Scale Effect, Confining Effect
Failure Type, Maximum Strength, Compressive Strength

1. INTRODUCTION

Recently, composite structure composed of concrete filled tube columns and wide-flange beams (CFT structure) has become more and more popular, since it has been proved by extensive experimental and theoretical investigation that CFT structure shows better performance in view of the strength, ductility, and energy dissipation than ordinary reinforced concrete, steel or steel-reinforced concrete structure. However, the scale effects on the behavior of the CFT members have been rarely investigated[1], although the scale effect on the compressive strength of plain concrete and confined concrete by lateral hoops has been investigated and clarified to a certain extent.

This paper first presents the results of compression tests of concrete cylinders encased by the steel tube, and compression tests of CFT short columns as a whole. Experimental variables were: i) shape of the cross section, ii) size of diameter or width, and iii) concrete strength. Then, discussed are the failure mode, strain distributions, load-deformation behavior and maximum strength in view of the scale effect. A formula to evaluate the compressive strength of a CFT short column considering the scale effect is presented, which has been derived from the analysis of the test results including the data presented elsewhere.

2. EXPERIMENTAL INVESTIGATION

2.1 Test Program

Table 1 shows the test program of centrally-loaded CFT short columns. Experimental parameters varied as follows: i) cross-sectional shape: circular and square, ii) nominal diameter D or width B of steel tube: 100, 200 and 300 mm, and iii) standard strength of concrete: F_c = 27, 36, 48 and 66 N/mm^2. Tubes were cold-formed steel tubes STK400 for circular section and STKR400 for square section. Cold-rolled tube BCR295 was used for the square section with width B = 300 mm. The class of diameter-thickness ratio of the circular section was FA, and that of the square section was FD in the classification of void tubes, where the ductility factor of 4 is guaranteed for the tube of FA class under the uniform compression, and the compressive stress of the tube of FD class cannot reach the yield stress since the local buckling occurs in the elastic range. Concrete was the normal concrete with Portland cement, in which coarse aggregates with the maximum size d = 20 mm were used. The cylinders have been cured without stripping until the day of the tests of centrally-loaded column conducted. The length of the specimen was 3 times the diameter or the width.

Table 1 Test Program of Centrally-Loaded CFT Short Columns

Shap	Steel grade	Diameter D [mm] Width B [mm]	Length h [mm]	Thickness t [mm]	D/t B/t	Class of D/t (B/t)	F_c [N/mm^2]	d [mm]	Test
① Circular	STK400	② 101.6	3D	3.2	31.8	③ FA	④ 27	20	⑤ A
		216.3		7.0	30.9		36		
		318.5		10.3	30.9		48		I
Square	STKR400	100.0	3B	2.3	43.5	FD	27		
		200.0		4.5	44.4		48		V
	BCR295	300.0		6.0	50.0		66		

F_c: standard strength of concrete d: maximum size of coarse aggregate

Test **A**: compression test of CFT short column as a whole

Test **I**: compression test of filled concrete encased in steel tube Test **V**: compression test of void tube

Legend for the name of specimen: **C10A-2A-1**
①②③④⑤⑥

① shape: **C** → Circular **S** → Square

② dismeter (width): **10** → D (B) = 100 [mm]

③ class of D/t (B/t): **A** → FA

④ standard strength of concrete: **2** → F_c = 27 [N/mm^2]

⑤ test method

⑥ identification number for identical specimens

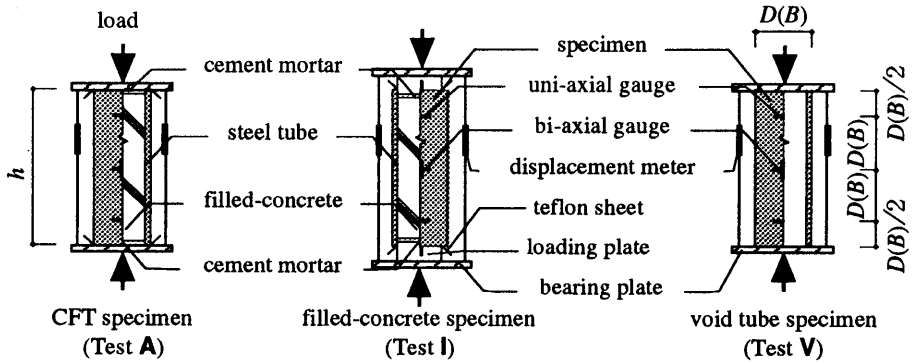

Fig. 1 Test Methods

Table 2 Test Results

(a) Void Tubes (Test V)

Specimen	$D\,(B)$ [mm]	t [mm]	D/t B/t	σ_y [N/mm²]	N_m [kN]	σ_{ym} [N/mm²]	σ_{ym}/σ_y
C10A-V	101.7	3.03	33.6	371	376	400	1.08
C20A-V	216.4	6.61	32.7	452	2126	488	1.29
C30A-V-1	318.4	10.36	30.7	331	3851	384	1.16
C30A-V-2	318.5	10.38	30.7	339	3758	374	1.10
S10D-V	100.1	2.18	45.9	300	249	295	0.98
S20D-V-1	200.1	4.35	46.0	322	984	293	0.91
S20D-V2	200.1	4.36	45.9	324	1006	299	0.92
S30D-V-1	300.6	6.10	49.3	395	2144	289	0.73
S30D-V-2	300.6	6.10	49.3	395	2195	296	0.75

(b) Concrete Cylinders Encased in Steel Tubes (Test I)

Specimen	$D\,(B)$ [mm]	σ_B [N/mm²]	N_m [kN]	σ_{ym} [N/mm²]	σ_{ym}/σ_B
C10A-2I-1	101.6	23.2	660	88.7	3.82
C10A-2I-2	101.8	23.2	649	94.3	3.87
C10A-2I-3	101.8	23.2	682	87.9	3.60
C20A-2I	216.5	24.3	3568	110.0	4.53
C30A-2I	318.5	24.2	6565	99.2	4.08
C10A-3I-1	101.6	40.2	800	120.7	3.00
C10A-3I-2	101.7	40.2	742	111.8	2.78
C20A-3I	216.5	38.2	4023	129.6	3.39
C30A-3I	318.4	39.2	7933	111.3	2.84
C10A-4I-1	101.5	51.3	877	120.3	2.35
C10A-4I-2	101.9	51.3	862	128.4	2.50
C20A-4I	216.4	46.8	4214	132.3	2.83
C30A-4I	318.3	52.2	8289	133.8	2.56
S10D-2I	100.2	25.7	411	45.0	1.75
S20D-2I	200.3	29.6	1613	44.1	1.49
S30D-2I	300.5	26.5	2766	33.4	1.26
S10D-4I	100.0	53.7	697	76.2	1.42
S20D-4I	200.1	57.9	2563	70.3	1.21
S30D-4I	300.6	58.9	5481	66.1	1.12
S10D-6I	101.1	61.0	783	85.6	1.40
S20D-6I	200.2	63.7	2825	77.4	1.22

(c) CFT (Test A)

Specimen	$D\,(B)$ [mm]	σ_B [N/mm²]	N_m [kN]	N_m/N_o
C10A-2A-1	101.4	23.2	660	1.29
C10A-2A-2	101.9	23.2	649	1.25
C10A-2A-3	101.8	23.2	682	1.32
C20A-2A	216.4	24.3	3568	1.29
C30A-2A	318.3	24.2	6565	1.31
C10A-3A-1	101.7	40.2	800	1.25
C10A-3A-2	101.3	40.2	742	1.17
C20A-3A	216.4	38.2	4023	1.25
C30A-3A	318.3	39.2	7933	1.30
C10A-4A-1	101.9	51.3	877	1.22
C10A-4A-2	101.5	51.3	862	1.20
C20A-4A	216.4	46.8	4214	1.21
C30A-4A	318.5	52.2	8289	1.17
S10D-2A	100.2	25.7	609	1.27
S20D-2A	200.3	29.6	2230	1.02
S30D-2A	300.5	26.5	5102	1.02
S10D-4A	100.1	53.7	851	1.15
S20D-4A	200.1	57.9	3201	1.00
S30D-4A	300.7	52.2	6494	0.91
S10D-6A	100.1	61.0	911	1.12
S20D-6A	200.3	63.7	3417	1.01

σ_y: yield stres σ_{ym}: maximum axial stress = N_m/A_s for Test **V**, and N_m/A_c for Test **I**

N_m: maximum laod N_o: squash load = $A_s \cdot \sigma_y + A_c \cdot \sigma_B$

A_s, A_c: areas of steel tube and concrete, respectively σ_B: cylinder strength

2.2 Test Methods

Figure 1 shows the loading methods schematically. Three kinds of compression tests have been conducted: i) Test **A**: CFT was centrally-loaded as a whole, ii) Test **I**: only the filled concrete encased in the tube was centrally-loaded, and iii) Test **V**: compression tests of void tube. Cement mortal was cast at the ends of specimens for Tests **I** and **A** to obtain the smooth surfaces subjected to the load, and two teflon sheets were insert between the loaded surface and bearing plate at both ends to remove the restraints of the plate on the lateral strain at the ends of the specimen. The change of the specimen length which was the change of the distance between two bearing plates were measured by two displacement meters, and longitudinal and circumferential strains of the steel tube were measured by bi-axial (longitudinal and circumferential) wire strain gauges mounted at the centers and uni-axial (circumferential) gauges mounted at the points of $D(B)/2$ apart from the ends. In Test **I**, only the filled-concrete was compressed using the loading plates whose diameter (width) was a little smaller than the steel tube encasing the concrete, and the longitudinal strain of the loading plates were measured by the wire strain gauges. The loading was terminated when the length change measured by the displacement meters became more than 6 % of the initial length.

3. TEST RESULTS AND DISCUSSION

Tables 2 (a) (b), and **(c)** show the test results: measured diameter D (width B) and thickness t, yield stress of steel tube σ_y, cylinder strength of concrete σ_B, the maximum compressive load N_m, and the maximum compressive strength $\sigma_{zm} = N_m/A_c$ or N_m/A_s, and the ratio of N_m of Test **A** to the squash load N_o, where $N_o = A_s \cdot \sigma_y + A_c \cdot \sigma_B$, A_s and A_c being cross-sectional areas of steel tube and concrete, respectively. The load kept increasing and the peak point did not appear during the tests of the specimens in **C__A-2I** series, and the maximum load listed in **Table 2** is the load value detected at the length change becoming 6 % of the original length.

3.1 Failure Mode

Photographs 1, 2 and **3** show the failure modes of specimens in Test **V**, **I** and **A**, respectively, each containing circular and square specimens.

Cross section of a circular void tube swelled out when the local buckling occurred as shown in **Photo. 1 (a)**, while two plate elements with welding seam of a square void tube dented inside, and another two without seam swelled out, as shown in **Photo. 1 (b)**.

Several lateral expansions were observed in a circular tube in Test **I** as shown in **Photo. 2 (a)**, and the positions of the expansion are apart some distance, from which it is observed that the diagonal slip may have occurred in the filled concrete. In the case of a square tube in Test **I**, the circumferential expansion occurred, and the cross section tended to be circular. Such expansion occurred within a failure region with length of l_p from the top, which was equal to about $2B$ in **S__D-2I** series, and about B in **S__D-4I** and **S__D-6I** series. The failure region was limited to the upper portion of the specimen, since the concrete in this region may have become weaker due to bleeding. The scale effect on the failure mode of the specimens in Test **I** was rarely observed in both circular and square tubes.

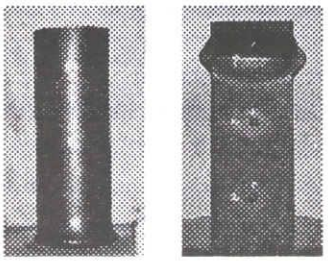

(a) Circular (b) Square

Photo. 1 Test V

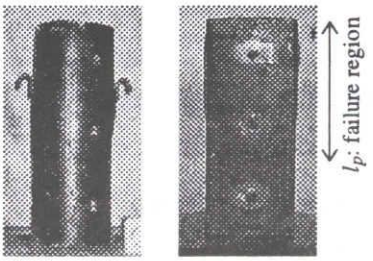

(a) Circular (b) Square

Photo. 2 Test I

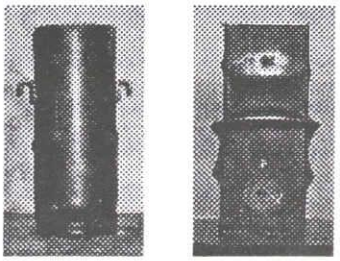

(a) Circular (b) Square

Photo. 3 Test A

The failure mode of a circular CFT in Test **A** was a combination of lateral expansion near the center with the local bucklings occurring at a little different heights, as shown in **Photo. 3 (a)**. In the case of a square CFT, a number of local buckling deformations occurred at different heights, as shown in **Photo. 3 (b)**, and the lateral expansion as observed in the specimen in Test **I** was not visibly observed.

3.2 Circumferential Strain Distributions

Figures 2 (a), (b) and **(c)** show distributions of the circumferential strain ε_θ changing with the progress of the length change ratio $\Delta h/h$ from 0.6 to 2.4 % with the interval of 0.3 %, which is the average of the data detected by four wire strain gauges mounted at each of the upper (U), center (C) and lower (L) positions. The value of ε_{zm} indicated in each figure is the axial strain data of the longitudinal gauge mounted at the center detected at the maximum load. Distributions indicated by solid circles and open circles were detected before and after the maximum load attained, respectively.

Circumferential strains of the specimen in Test **V** shown in **Fig. 2 (a)** uniformly distributed and increased before the maximum load attained with the occurrence of local buckling, but then they stopped increasing, since the deformation concentrated to the locally-buckled position which was different from the position at the wire strain gauges mounted.

In the case of a circular specimen **C20A-2I** in Test **I**, circumferential strain at the center became the largest, because of the lateral expansion occurring at the center. The strain at the upper position became larger than that at the lower position in the case of **C20A-4I**, maybe because of the weak concrete due to bleeding, as mentioned before in relation to the failure mode of the circular specimen in Test **I**. The effect of weak concrete at the upper layer due to bleeding is more pronounced in the square specimens in Test **I**. Especially, the strains at the center and the lower layer of **S10A-4I** rarely increased after the maximum load, and this means that the failure occurred only in the upper layer.

Strain concentration to the center layer was observed in the circular specimens in Test **A** as observed in those in Test **I**, in addition to the progress of the strains at all layers. Failure concentration was observed in the square specimens in Test **A**: concentration to the center layer of **S30A-2A** due to the local buckling, and to also the upper layer of **S30A-4A** due to bleeding.

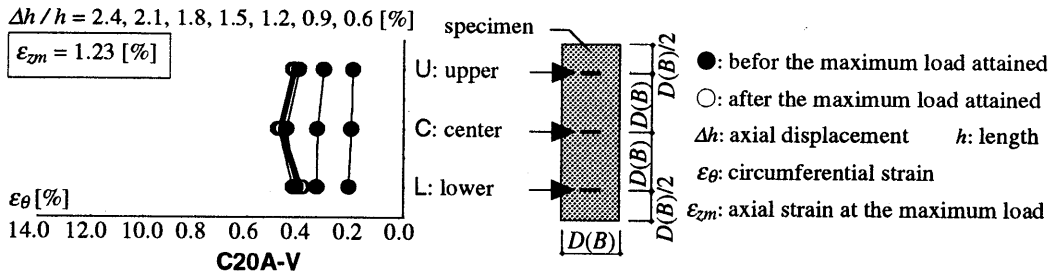

(a) Void Tubes (Test V)

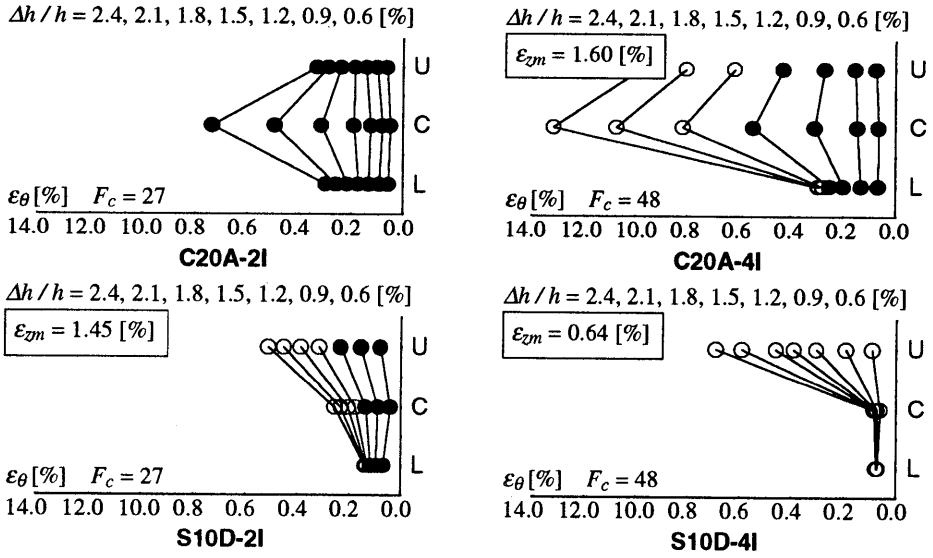

(b) Concrete Cylinders Encased in Steel Tubes (Test I)

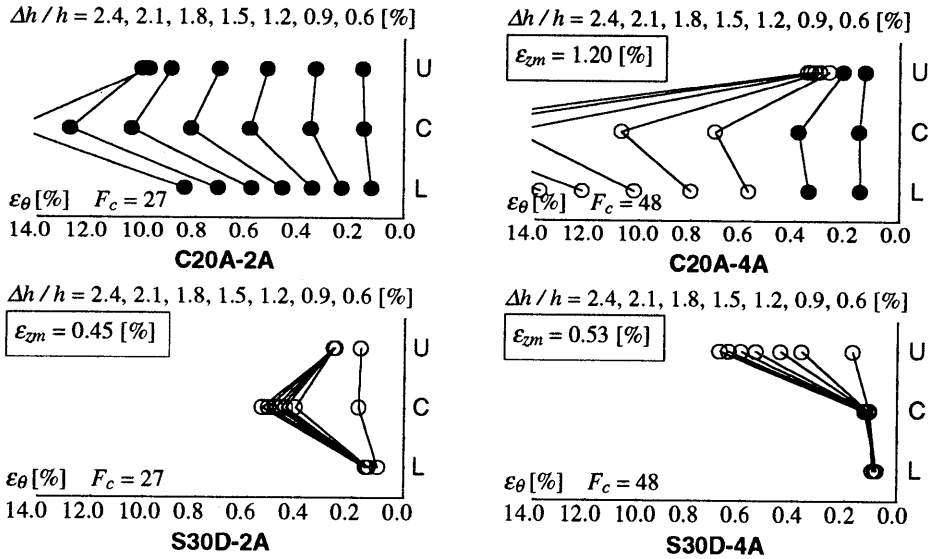

(c) CFT (Test A)

Fig. 2 Distributions of Circumferential Strains

3.3 Load-Deformation Behavior

Test I **Figures 3 (a)** and **(b)** show the relations between the longitudinal stress σ_z (= N/A_c) divided by the cylinder strength σ_B and the length change ratio $\Delta h/h$, obtained from Test **I**. Solid triangle indicates the peak point on the curve. It is observed from the figure that the maximum value of the stress ratio σ_{zm}/σ_B becomes smaller and the slope of the unloading curve becomes steeper, as the concrete strength increases. This is because the confining effect of steel tube becomes relatively smaller as the concrete strength becomes higher, since the effective lateral pressure provided by the tube does not change among the specimens with the same value of D/t and σ_y. With the same reason of relatively small lateral pressure, the maximum value of the stress ratio of the specimens in Test **I** is larger than that in Test **A**, since the steel tube in the former is fully used for the confinement only, while that in the latter carries the longitudinal stress in addition.

As to the scale effect, it is obviously appearing in the results of square specimens: the maximum value of the stress ratio becomes smaller as the width becomes larger. However, the scale effect on the circular specimens is not clear. The maximum value of the stress ratio of **C20A-_I** is larger than **C10A-_I** and **C30A-_I**, regardless of the concrete strength, since the effective lateral pressure in the case of the circular specimens with diameter equal to 200 mm was the largest due to the strongest steel material used.

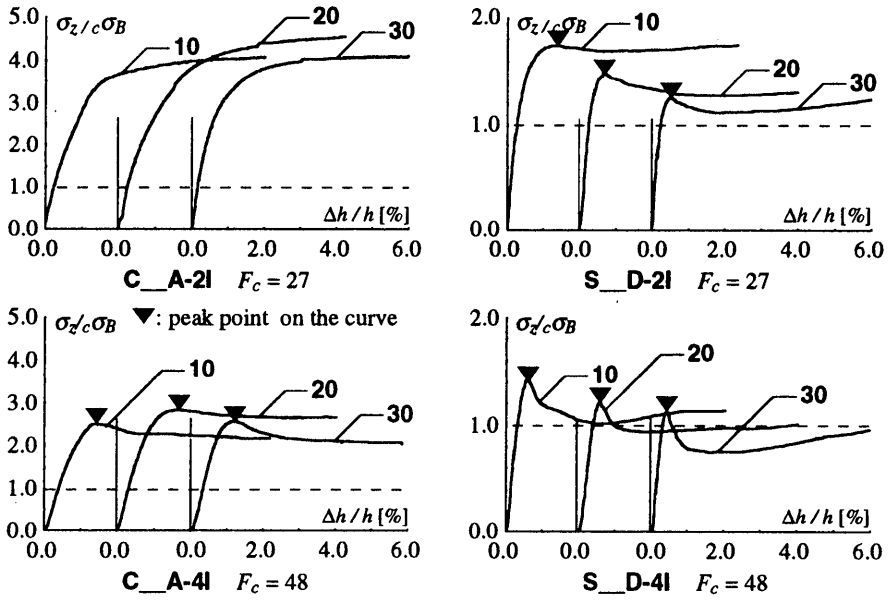

Fig. 3 Relations between Axial Stress and Axial Deformation (Test I)

Test A **Figures 4 (a)** and **(b)** shows the relation between the compression load N divided by the squash load N_o and the length change ratio $\Delta h/h$, obtained from Test **A**. Solid triangles indicate the points of the maximum load attained, and open triangles indicate the value of $\Delta h/h$ at which the maximum load was observed in Test **V** of the corresponding specimens with the same diameter or the width. In the case of circular specimens, tendencies are observed that the maximum value of the load ratio becomes smaller as the concrete strength becomes higher, and

the deformation indicated by the solid triangle is larger than that by the corresponding open triangle in the case of the specimens in **C__A-2A**, while that is smaller in the case of the specimens in **C__A-4A** series. These tendencies are because of brittle failure observed in the specimen made of the concrete with higher strength: The concrete with higher strength fails in more brittle manner in the earlier stage, which tries to expand the tube from the inside, and then triggers the local buckling. On the other hand, the deformation indicated by the solid triangle is always larger than that of the corresponding open triangle in the square specimens, which is caused by the difference in the mode of local buckling: the plate element of a void tube shows the pinned-pinned mode, while that of a CFT shows the clamped-clamped mode, and thus the occurrence of the latter is delayed. The scale effect is clearly observed again in the square specimens as observed in Test **I**, but it is not very clear in the circular specimens.

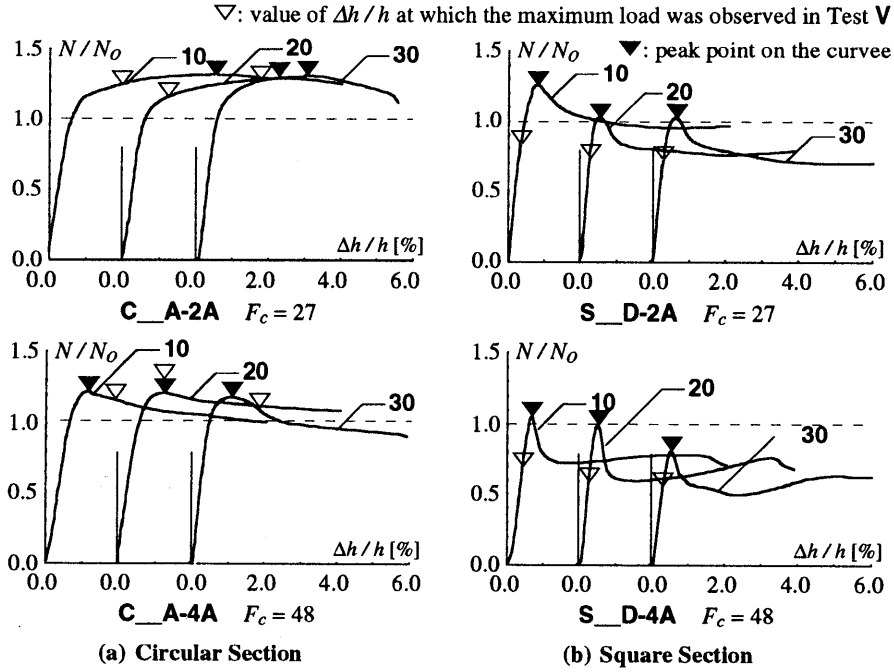

Fig. 4 Relations between Axial Load and Axial Deformation (Test A)

3.4 Maximum Strength of Confined Concrete (Test I)

Effect of Concrete Strength In **Figs. 5 (a)** and **(b)**, the values of K/K_o are plotted against the values of σ_B, to show the effect of concrete strength on the strength of the specimen in Test **I**, where $K = \sigma_{zm}/\sigma_B$, σ_{zm} = maximum compressive strength obtained from the Test **I**, σ_B = cylinder strength, and K_o is the value of K of the specimen with $\sigma_B \fallingdotseq 27$ N/mm^2. Solid marks are the results of present tests, and open marks are the test results collected from the literatures. The thick line is a hyperbolic type empirical formula derived by a regression analysis of the test data. The value of K/K_o reduces with the increase in the concrete strength, and the reduction rate for the circular specimens is a little steeper than that for the square specimens.

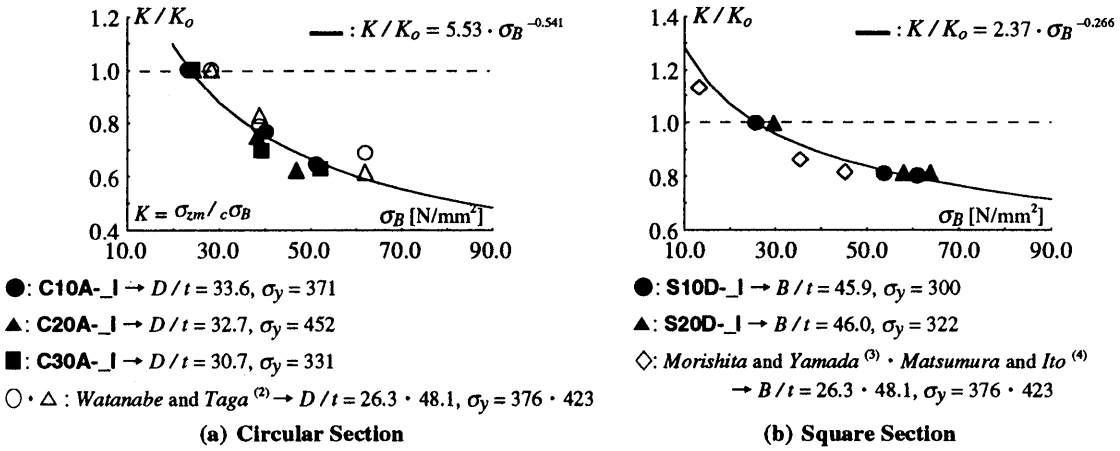

(a) Circular Section **(b) Square Section**

Fig. 5 Effects of Concrete Strength (Test I)

Scale Effect In **Fig. 6**, the values of K/K_1 are plotted against the values of A_c, to show the scale effect on the strength of the specimen in Test **I**, where K_1 is the value of K of the specimen with D or $B \fallingdotseq 100$ mm. Solid marks are the test results of circular specimens, and open marks are the results of square specimens. The curve is an empirical formula derived by *Blanks* and *McNamara*[5] for plain concrete cylinders. The original formula proposed by *Blanks and McNamara* was for circular cylinders, and written in terms of the diameter of the cylinder, but the original formula was converted to the one written in terms of the concrete area, so that it can be applied to the square cylinders. Mathematical expressions of the original and converted formulas are given as follows:

$$\sigma_{Bp} = 1.67 \cdot D^{-0.112} \cdot \sigma_B \rightarrow \sigma_{Bp} = 1.65 \cdot A_c^{-0.056} \cdot \sigma_B \qquad (1)$$

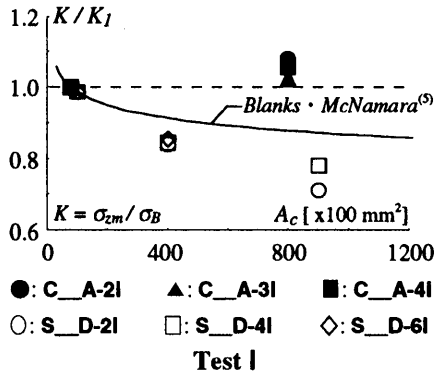

Test I

Fig. 6 Effects of Specimen Size

The scale effect on the circular specimens is not clear, as mentioned in Sect. 3.3, while it clearly appears in the case of square specimens, and the strength reduction due to the increase in the size is larger than that of the plain concrete, since the confinment in the square CFT relatively reduces as the size increases, which will be discussed in detail later.

3.5 Axial Stress-Circumferential Strain Relation (Test I)

The relations between the stress ratio σ_z/σ_B and the circumferential strain ε_θ of the specimens in Test I are given in **Fig. 7**, the value of ε_θ being the average of the data of 4 strain gauges mounted on the square tube at the upper layer U in **Fig. 2(a)**. Solid lines indicate the test results of **C__A-2I** or **S__A-2I** series, and dashed lines indicate **C10A-_I** or **S10A-_I** series. Solid triangles indicate the peak points.

In the case of circular specimens shown in **Fig. 7(a)**, The scale effect is not clearly observed, and the strength ratio becomes smaller as the concrete strength increases, since the confinment becomes relatively smaller with the increase in the concrete strength. On the other hand, a tendency is observed from **Fig. 7(b)** for square specimens that the circumferential strain at the maximum load becomes smaller as the size of the specimen becomes larger, or the concrete strength becomes higher. The stiffness of the plate of the square tube which confines the filled concrete becomes smaller as the width of the tube becomes larger. This is the main reason of the scale effect on the strength reduction of the square specimen of Test I.

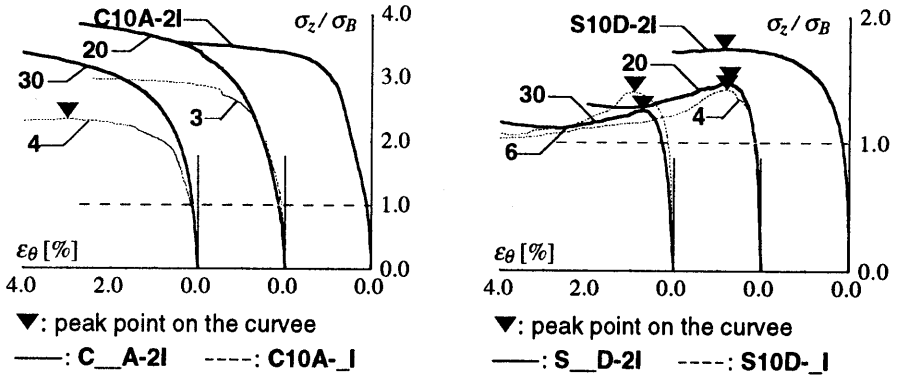

(a) Circular Section (b) Square Section

Fig. 7 Relations between Axial Load and Perimeter Strain of square Tubes (Test I)

4. EVALUATION OF COMPRESSIVE STRENGTH

4.1 Strength Evaluation of Confined Concrete (Test I)

Previously-Proposed Formulas Evaluation formula for the compressive strength of confined concrete σ_{Bc} was proposed by *Richart*[6], which was written in terms of the cylinder strength σ_B and lateral restraining stress σ_r, as follows:

$$\sigma_{Bc} = \sigma_B + k \cdot \sigma_r \tag{2}$$

Tomii and *Sakino*[7] and *Matsumura* and *Ito*[4] proposed Eqs. (3) and (4) to evaluate σ_r for the filled concrete confined by the circular and square tubes, respectively.

$$\text{circular cylinder: } \sigma_r = \frac{2t}{D-2t}\sigma_y \tag{3}$$

square cylinder: $\sigma_r = 4\,(t/B)^2 \cdot \sigma_y$ (4)

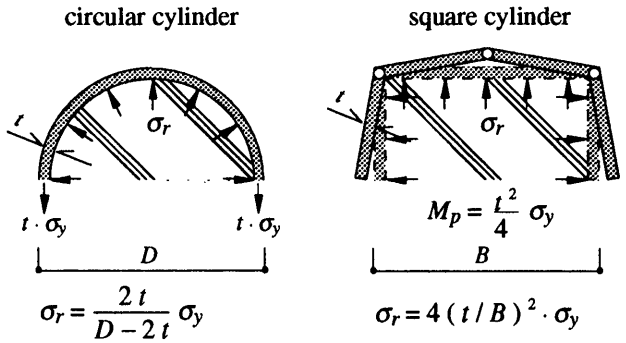

(a) Circular Section (b) Square Section

Fig. 8 Models for Confinement

Equation (3) was derived from the equilibrium shown in **Fig. 8 (a)**: equilibrium between lateral (confining) stress σ_r and circumferential stress which is assumed to be equal to σ_y. Equation (4) was based on the collapse mechanism shown in **Fig. 8 (b)**: three plastic hinges with the plastic moment M_p form in the tube wall with a unit width under lateral stress σ_r. Lateral stress σ_r is the reaction from the concrete, and it confines the concrete.

Equations (2) may be converted by replacing σ_B by σ_{Bp} to consider the scale effect, and finally the compressive strength of confined concrete filled in circular or square tubes may be given as follows:

circular cylinder: $\sigma_{Bc} = \sigma_{Bp} + k \dfrac{2t}{D-2t}\sigma_y$ (5)

square cylinder: $\sigma_{Bc} = \sigma_{Bp} + k \cdot 4\,(t/B)^2 \cdot \sigma_y$ (6)

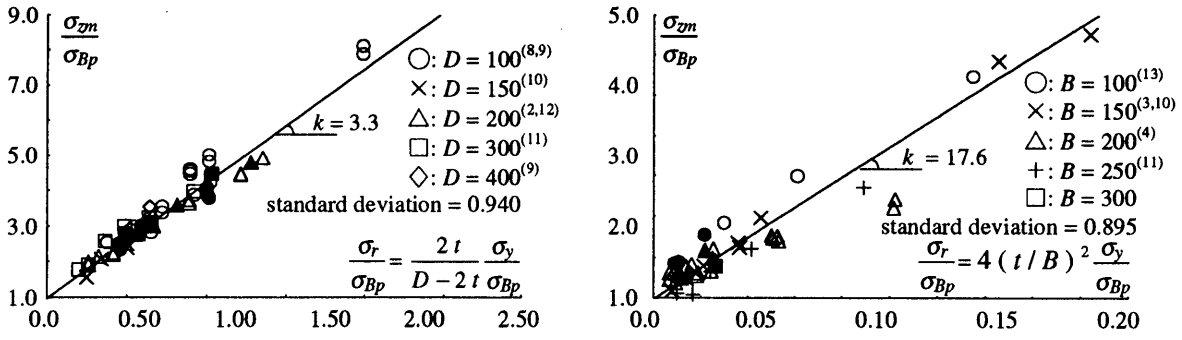

(a) Circular Section (b) Square Section

Fig. 9 Evaluation of Confining Factor k (Test I)

In **Figs. 9 (a)** and **(b)**, the values of σ_{zm}/σ_{Bp} obtained from Test **I** are plotted against the values of σ_r/σ_{Bp}, in which σ_r was evaluated by Eqs. (3) and (4). Solid marks indicate the present test data, and open marks the data found in the literatures[2-4,8-13]. Straight lines were obtained by the regression analysis of the data using the least squares method, whose inclination angle gives the value of confining factor k. The values of k = 3.3 and 17.6 were obtained for the circular and square specimens, respectively.

In **Fig. 10**, the values of σ_{zm}/σ_{Bc} are plotted against the size, where the values of σ_{Bc} are calculated by Eqs. (5) and (6) with k =3.3 and 17.6 for circular and square specimens, respectively. It becomes known that the accuracy of Eq. (5) is sufficient, while that of Eq. (6) is not very good.

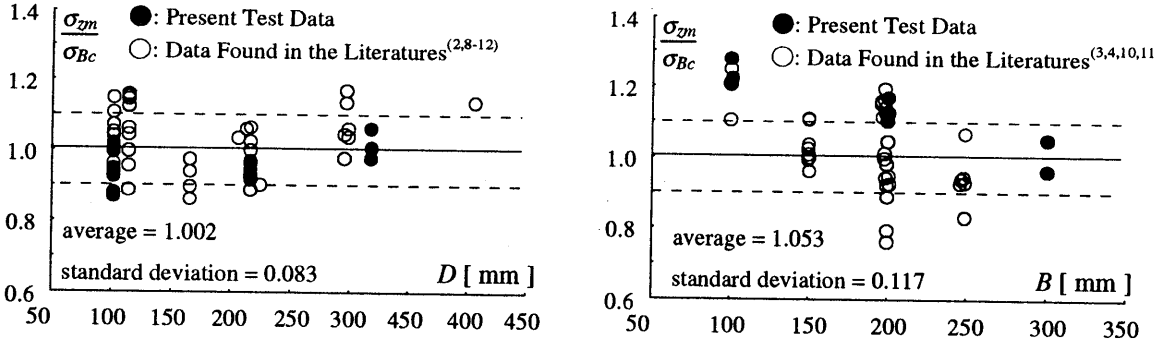

Fig. 10 Evaluation of Compressive Strength of Filled-Concrete Specimens (Test I)

Newly-Proposed Formula for Concrete Confined by Square Tube In the previous discussion, it has been clarified that the strength of confined concrete in a circular CFT is well estimated, but a more accurate formula is needed to estimate the strength of confined concrete in a square CFT. In this section, a new formula is proposed, which takes the effect of the width of the square CFT into consideration.

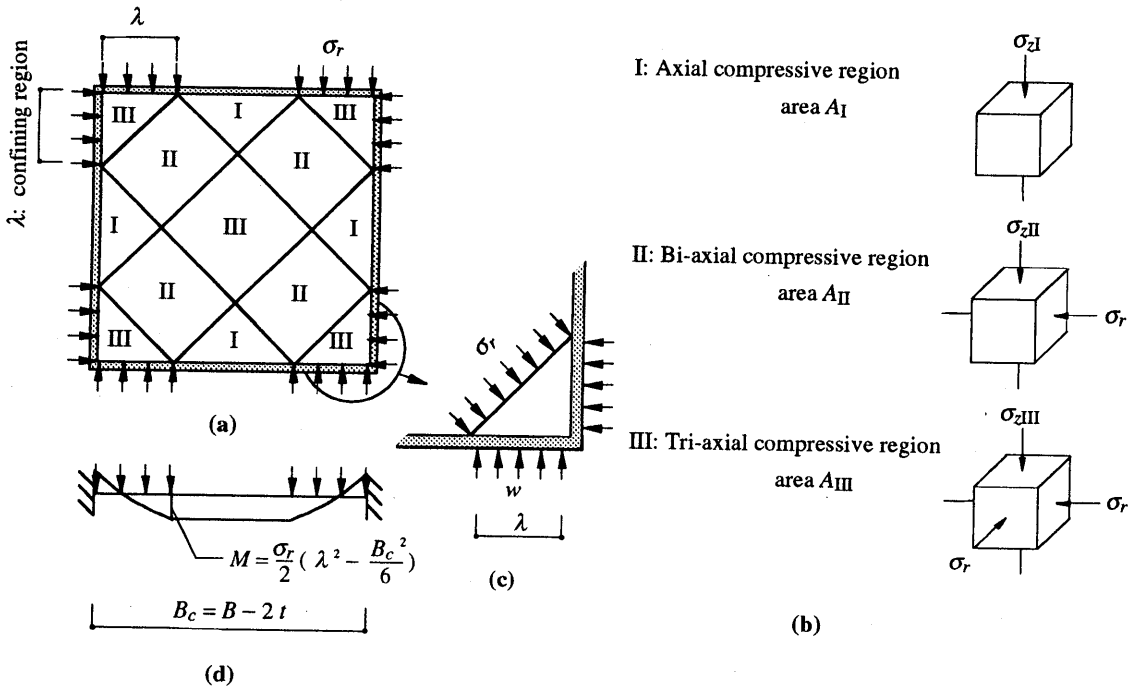

Fig. 11 Confining Region and Zoning of Square Concrete Area [4][14]

The internal pressure of square CFT may be mainly carried in the corner region as shown in **Fig. 11(a)**, rather than the uniform distribution shown in **Fig. 8 (b)**. This consideration explains the reason why the strength of square CFT decreases with the increase in the width. The model in **Fig. 11(b)** assumes 3 kinds of state of stress: the concrete in the area A_I carries the axial compression σ_z only without confinement, and the compressive strength σ_{zmI} of this area is given by Eq. (7) considering the size effect for the plain concrete; the concrete in A_{II} is subjected to σ_z and uni-directional lateral stress σ_r, and σ_{zmII} in this area is given by Eq. (8), which was proposed by *Fan* and *Shiiba*[14]; and the concrete in area A_{III} is subjected to σ_z and bi-directional lateral stress σ_r. The compressive strength σ_{zmIII} in the area A_{III} is assumed to be given by Eq. (9), as proposed by Richart[6] , in which k is taken equal to 3.3, considering that the state of stress in A_{III} is similar to that of the concrete in the confined circular cylinder.

$$\sigma_{zmI} = \sigma_{Bp} = 1.65 \cdot A_c^{-0.056} \cdot \sigma_B \tag{7}$$

$$\sigma_{zmII} = 0.5\ \sigma_{Bp}\ (\ 1.0 + \sqrt{1.0 + 10.6\ \sigma_r / \sigma_{Bp}}\ ) - \sigma_r \tag{8}$$

$$\sigma_{zmIII} = \sigma_{Bp} + k \cdot \sigma_r \qquad k = 3.3 \tag{9}$$

The lateral stress was evaluated in the following manner. The lateral stress σ_r working on the block A_{II} is supported by the pressure w at the corner uniformly distributed along the distance λ, as shown in **Fig. 11(c)**. From the equilibrium of a right-angled equilateral triangle element with the size of λ and unit thickness, it becomes known that $w = \sigma_r$. It is assumed that the pressure w causes bending moment and axial tension in the tube wall, which is modelized to an elastic clamped beam with length B_c (= $B - 2t$) made of a rectangular cross section of depth t and a unit width, as shown in **Fig. 11(d)**. Noting that $w = \sigma_r$, the largest bending moment M and axial tension N are given by

$$M = \frac{\sigma_r}{2}\left(\lambda^2 - \frac{B_c^{\,2}}{6}\right) \tag{10}$$

$$N = \sigma_r \cdot \lambda \tag{11}$$

The axial tension N is in equilibrium with the pressure working at the side wall of the tube. Finally, the lateral stress was determined on the assumption that it causes the first plastic hinge in the beam. Substituting M and N given by Eqs. (10) and (11) into the full plastic condition for a rectangular section

$$\frac{M}{M_p} + \left(\frac{N}{N_y}\right)^2 = 1 \tag{12}$$

leads to the following equation, which determines the value of σ_r:

$$\left(\frac{\sigma_r}{\sigma_y}\right)^2 + \left\{6 - \left(\frac{B_c}{\lambda}\right)^2\right\}\left(\frac{\sigma_r}{3\,\sigma_y}\right) - \left(\frac{t}{\lambda}\right)^2 = 0 \tag{13}$$

The calculated ultimate compressive load and corresponding axial stress of the square filled concrete in Test I are given by

$$N_u = \sum_{i=\mathrm{I,\,II,\,III}} A_{ci} \cdot \sigma_{zmi}\,; \qquad \sigma_{Bc} = \frac{N_u}{A_c} \tag{14}$$

The values of the length λ of confining region was empirically determined by equating N_u of Eqs. (14) to the maximum load N_m obtained in the tests, and they are plotted against the values of the concrete size B_c in **Fig. 12**. The regression analysis by the least squares gives an empirical formula

$$\lambda = 0.44\,B_c - 1.96 \tag{15}$$

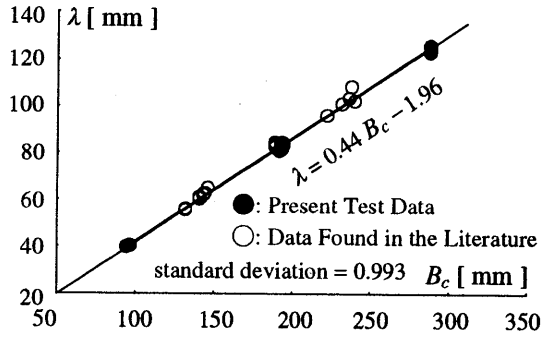

Fig. 12 Evaluation of Confining Region λ (Test I)

In **Fig. 13**, the values of σ_{zm}/σ_{Bc} are plotted against the width B, where the values of σ_{Bc} are calculated by Eq. (14) together with Eqs. (7) through (9), (13) and (15). Strength estimation becomes much better than that shown in **Fig. 10(b)**, most data being within the error of ±10%.

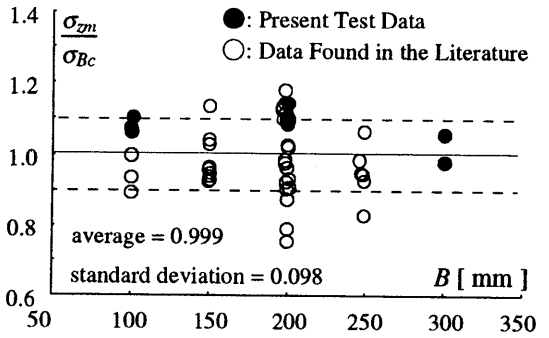

Fig. 13 Evaluation of Compressive Strength of Filled-Concrete Specimens (Test I)

4.2 Strength Evaluation of CFT Short Columns (Test A)

Previously-Proposed Formulas Formulas to evaluate the compressive strength of a centrally-loaded CFT short column were proposed in *Ref.* (15) based on the test data obtained in the US-Japan Cooperative Earthquake Research Program, as follows:

circular CFT: $N_u = 1.27\, A_s \cdot \sigma_y + A_c \cdot \sigma_B$ (16)

square CFT: $N_u = A_s \cdot \sigma_{cr} + A_c \cdot \sigma_{Bp}$ (17)

$$\sigma_{cr} = \sigma_y \quad \text{for} \quad \frac{B}{t} \le 1.5\ \frac{74}{\sqrt{\sigma_y}}$$

$$\sigma_{cr} = S \cdot \sigma_y \quad \text{for} \quad \frac{B}{t} > 1.5\ \frac{74}{\sqrt{\sigma_y}}$$

$$\text{press-formed square tube: } \frac{1}{S} = 0.698 + 0.128 \cdot \left(\frac{B}{t}\right)^2 \cdot \frac{\sigma_y}{E_s} \cdot \frac{4.00}{6.97}$$

$$\text{roll-formed square tube: } \frac{1}{S} = 0.778 + 0.130 \cdot \left(\frac{B}{t}\right)^2 \cdot \frac{\sigma_y}{E_s} \cdot \frac{4.00}{6.97}$$

Equation (16) was empirically obtained from the test data, and Eq. (17) is also an empirical formula, in which the strength reduction of the tube due to local buckling is considered. The limit value of B/t ratio is relaxed to 1.5 times the value for the void tube. Formulas for the strength reduction factor S is converted from the formulas for the void tube considering the difference of the buckling mode of a rectangular plate subjected to uniform compression: the value 4.00 is for the buckling coefficient of a plate supported by pinned-pinned condition, while 6.97 is for a plate supported by clamped-clamped condition.

In **Figs. 14 (a)** and **(b)**, the values of the maximum load N_m obtained in the tests are compared with those of N_u calculated by Eqs. (16) and (17). Accuracy of Eq. (16) for circular CFT is very good: most data are within the error of $\pm 10\%$. The estimation of the strength of square CFT by Eq. (17) is not so bad, although confining effect is not considered.

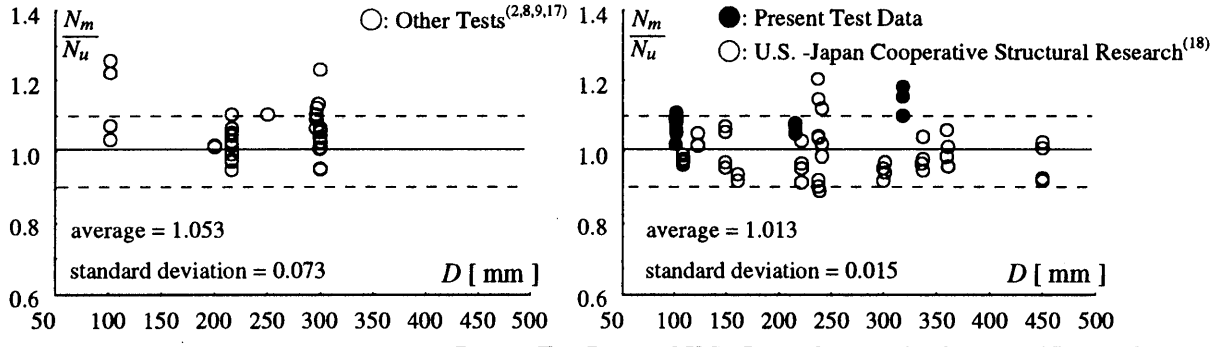

Data Found in the Literatures **Present Test Data and U.S. -Japan Cooperative Structural Research**

(a) Circular Section

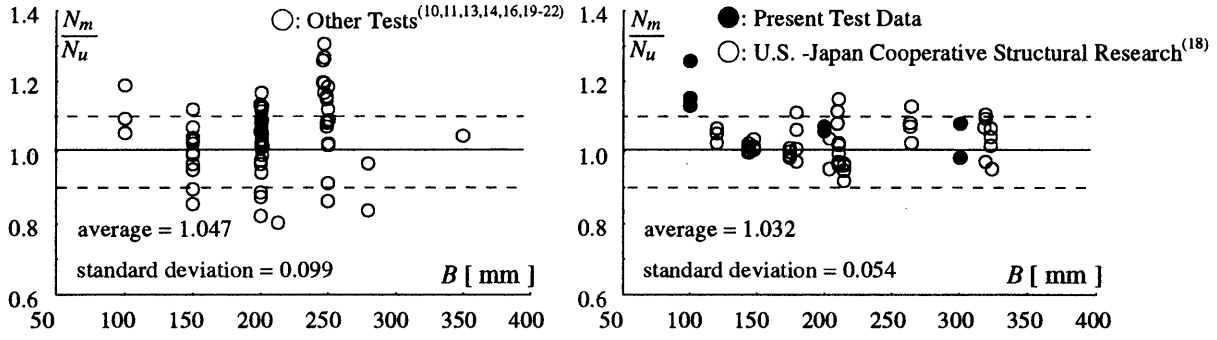

Data Found in the Literatures **Present Test Data and U.S. -Japan Cooperative Structural Research**

(b) Square Section

Fig. 14 Evaluation of Compressive Strength of CFT Short Columns (Test A)

Newly-Proposed Formula for Square CFT Short Columns In the case of Test **A**, the steel tube somewhat confines the filled-concrete, and the circumferential stress is generated as a reaction of confinement, which leads to the reduction of compressive strength. Since there have been very few data about the circumferential stress of a square CFT, the data obtained from the present tests were analyzed. **Figure 15(a)** shows the stress trajectories calculated from the wire strain gauge data for the circumferential and axial strains obtained in Test **A** of square CFT specimens, together with *Von Mises* yield criterion. The average value of $\alpha = \sigma_z/\sigma_y$ was obtained as 0.96, which is a little higher than 0.94 shown in *Ref.* (15). The value of $\beta = \sigma_\theta/\sigma_y$ corresponding to $\alpha = 0.96$ is then determined from *Von Mises* yield criterion shown in **Fig. 15(b)** as $\beta = -0.08$.

sign	Name of Specimen	σ_z / σ_y
○	**S10D-2A**	1.00
△	**S20D-2A**	0.96
□	**S30D-2A**	0.97
●	**S10D-4A**	0.97
▲	**S20D-4A**	0.91
	average	0.96

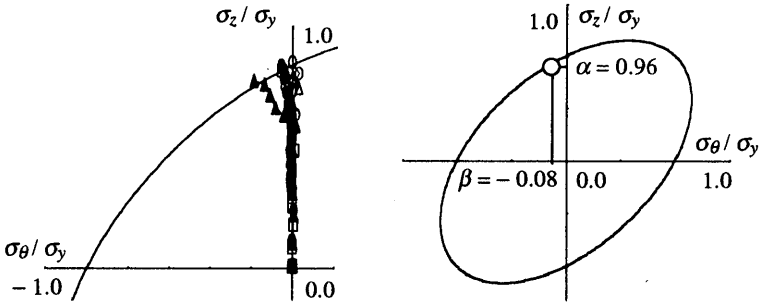

(a) (b)

Fig. 15 *Von Mises* Yield Criterion and Biaxial State of Stress (Test A)

Based on the same consideration to derive the lateral (confining) stress σ_r shown in Eq. (13) for the concrete encased in square tube, Eq. (13) may be used to evaluate σ_r for the concrete in a square CFT short column, by replacing σ_y by $\beta \cdot \sigma_y$, that is,

$$\left(\frac{\sigma_r}{\beta \cdot \sigma_y}\right)^2 - \left\{6 - \left(\frac{B_c}{\beta \cdot \lambda}\right)^2\right\}\left(\frac{\sigma_r}{3\beta \cdot \sigma_y}\right) - \left(\frac{t}{\beta \cdot \lambda}\right)^2 = 0; \quad \beta = -0.08 \tag{18}$$

Finally, The ultimate compressive load of a square CFT short column is calculated by

$$N_u = A_s \cdot \sigma_{cr} + \sum_{i\,=\,\mathrm{I,\,II,\,III}} A_{ci} \cdot \sigma_{zi}; \tag{19}$$

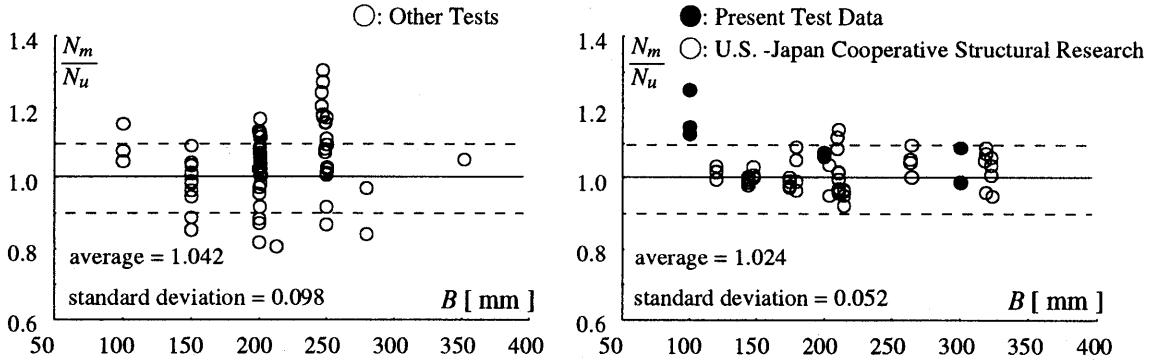

Data Found in the Literatures **Present Test Data and U.S. -Japan Cooperative Structural Research**

Fig. 16 Evaluation of Compressive Strength of CFT Short Columns (Test A)

where σ_{zi} are calculated by Eqs. (7) through (9) in view of σ_r determined by Eq. (18) with Eq. (15), and σ_{cr} by Eq. (17) with replacing σ_y by $\alpha \cdot \sigma_y$, where $\alpha = 0.96$.

The values of N_m are compared with those of N_u calculated by Eq. (19) in **Fig. 16**. Comparison between **Figs. 14** and **16** shows that the accuracy of evaluation formula is a little improved. The question is left for the future investigation; whether or not it is pertinent to include the effects of confined concrete and local buckling at the same time.

CONCLUSIONS

Compression tests of concrete cylinders encased in steel tubes and CFT short columns have been carried out, and the following findings have been obtained:

1) Scale effects on square CFT were observed, while those on circular CFT were not clearly observed.

2) Confining effect on the concrete strength was also observed in square CFT short columns.

3) The ultimate compressive strength of circular CFT is fairly accurately evaluated by the formulas proposed in the earlier literatures[7][15].

4) Strength formula for square CFT short column proposed in this study fairly well evaluates the strength obtained in the tests.

ACKNOWLEDGEMENTS

The steel tubes used in the tests were cordially provided by Kozai Club. The tests of larger specimens were done in the laboratories of Aichi Institute of Technology and NKK corporation, with the assistance of *Prof. Sachio Koike* of AIT and *Mr. Hiroumi Shimokawa* of NKK. The authors wish to express their sincere gratitude to those who helped this experimental study.

REFERENCES

(1) T. Sato: *Confining Mechanism and Analytical Model in Circular Concrete-Filled Steel Tube under Axial Force*, Transaction of Architectural Institute of Japan (AIJ), Journal of Structural and Construction Engineering, No. 452, pp. 149-158, 1993. 10 (in Japanese)

(2) T. Watanabe, A. Taga and S. Iwaoka: *Development of Concrete Filled Steel Tubular Structure (Part 4)*, Summaries of Technical Papers of Annual Meeting, AIJ, Structure II, pp. 1735-1736, 1993. 9 (in Japanese)

(3) Y. Morishita, Y. Yamada and A. Shimabukuro: *Experimental Studies on Load-carrying Capacity of Concrete Core Confined by Square Steel Tubes*, Summaries of Technical Papers of Annual Meeting, AIJ, Structure II, pp. 1571-1572, 1991. 9 (in Japanese)

(4) H. Matsumura and S. Ito: *Compressive Strength of Filled Concrete in Square Steel Pipe*, Summaries of Technical Papers of Annual Meeting, AIJ, Structure II, pp. 1627-1628, 1989. 10 (in Japanese)

(5) R. F. Blanks and C. C. McNamara: *Mass Concrete Tests in Large Cylinders*, Jour. of ACI, Vol. 31, No. 3, pp. 280-303, 1935. 1-2.

(6) F. E. Richart, A. Brandzaeg and R. L. Brown: *The Failure of Plain and Spirally Reinforced Concrete in Compression*, Bulletin No. 190, University of Illinois, Engineering Experimental Station, Urbana, 1929.2.

(7) M. Tomii and K. Sakino: *Present Condition of Study on the Concrete Filled Steel Structure*, Concrete Journal, Vol. 13, No. 2, pp. 26-41, 1975. 2 (in Japanese)
(8) K. Sakino, K. Watanabe and M. Tomii: *Experimental Studies on the Design Method to Prevent the Shear Failure of Reinforced Concrete Short Columns by Using Steel Tube, Part 2 Sustaining Load Capacity of Stub Columns*, Summaries of Technical Papers of Annual Meeting, AIJ, Structure II, pp. 415-416, 1985. 10 (in Japanese)
(9) T. Sato, H. Nakajima Y. Orito T. Ito N. Tanaka Y. Saito K. Nakamura H. Shiokawa Y. Orito Y. Watanabe and T. Tezuka: *Study on the Unbond Tubular Steel Encased Concrete Beam Columns Part 1-3*, Summaries of Technical Papers of Annual Meeting, AIJ, Structure II, pp. 1417-1422, 1986. 8 (in Japanese)
(10) I. Yamaguchi, S. Kanno T. Nagashima T. Hirade and H. Sawadal: *An Experimental Study on the Behavior of Concrete Filled Steel Tubular Columns under Uni-Axial Load, Part 1-2*, Summaries of Technical Papers of Annual Meeting, AIJ, Structure II, pp. 1353-1356, 1988. 10 (in Japanese)
(11) A. Kadono, Y. Saito, I. Yamaguchi T. Matsutani H. Matsumura and T. Yamaguchi: *A Study on the Behavior of Concrete Filled Steel Tubular Columns, Part 1-2*, Summaries of Technical Papers of Annual Meeting, AIJ, Structure II, pp. 1613-1616, 1989. 10 (in Japanese)
(12) H. Hirayama, K. Fukuda, and Y. Ichie: *Axial Compression Behavior of Concrete Filled Circular Column Made of 60 kg/mm² Tensile Strength Steel Tube, Part 1-2*, Summaries of Technical Papers of Annual Meeting, AIJ, Structure II, pp. 1797-1800, 1993. 9 (in Japanese)
(13) H. Yoshitomi, S. Morino, and J. Kawaguchi: *Experimental Study on the Stress-Strain Relation of Concrete Filled Steel Tubes*, Summaries of Technical Papers of Annual Meeting, AIJ, Structure II, pp. 1573-1574, 1994. 9 (in Japanese)
(14) Z. Fan and K. Shiiba: *Experiment Study on Concrete-Filled Steel Tubular Column, Part 6*, Summaries of Technical Papers of Annual Meeting, AIJ, Structure II, pp. 1627-1628, 1993. 9 (in Japanese)
(15) *Guideline for the Structural Design of CFT Column System (Draft)*, Building Research Institute, Ministry of Construction, 1998. 8 (in Japanese)
(16) T. Suzuki, S. Motoyui and H. Ohta: *Buckling and Post Buckling Behavior of Concrete Filled Rectangular Steel Tubular Stub Columns Under Pure Axial Compression*, Transaction of AIJ, Journal of Structural and Construction Engineering, No. 486, pp. 143-151, 1996. 8 (in Japanese)
(17) T. Suzuki, S. Motoyui and H. Ohata: *Study on Structural Properties of Concrete Filled Circular Steel Tubular Stub Columns Under Pure Axial Compression*, Transaction of AIJ, Journal of Structural and Construction Engineering, No. 499, pp. 123-129, 1997. 9 (in Japanese)
(18) T. Fujimoto, A. Mukai, I. Nishiyama, E. Inai, M. Kai, Y. Tanaka, H. Tokinoya, T. Noguchi, T. Baba, N. Fukumoto, Y. Murata, K. Sakino and S. Morino: *Axial Compression Behavior of Concrete Filled Steel Tubular Stub Columns Using High Strength Materials*, Transaction of AIJ, Journal of Structural and Construction Engineering, No. 498, pp. 161-168, 1997. 8 (in Japanese)
(19) T. Suzuki, M. Kimura T. Ogawa H. Ito and S. Miyashita: *Elasto-Plastic Behaviors of Concrete-Filled Square Steel Tubular Columns*, Transaction of AIJ, Journal of Structural and Construction Engineering, No. 345, pp. 70-77, 1984. 11 (in Japanese)
(20) H. Ge and T. Usami: *Strength of Concrete-Filled Thin-Walled Steel Box Columns, Experiment*, Journal of Structural Engineering, ASCE, Vol. 118, No. 11, pp. 3036-3054, 1992. 11
(21) T. Taguchi, N. Hayashi: *A Study on the Behavior of Concrete Filled Steel Tubular Columns using High-Strength Materials under Axial Load, Part 1-2*, Summaries of Technical Papers of Annual Meeting, AIJ, Structure II, pp. 1793-1796, 1993. 9 (in Japanese)
(22) H. Nakahara and K. Sakino: *Axial Compressive Test of High Strength Concrete Filled Square Steel Tubular Columns*, Summaries of Technical Papers of Annual Meeting, AIJ, Structure III, pp. 1131-1132, 1998. 9 (in Japanese)